Progress In Electromagnetics Research M, Vol. 81, 127–136, 2019

Achieving the Constant Output Power and Transfer Efficiency of a Magnetic Coupling Resonance Wireless Power Transfer System Based on the Magnetic Field Superposition Principle

Suqi Liu[1, 2, *], Jianping Tan[2], and Yuping Liu[1]

Abstract—The output power of a magnetic coupling resonance wireless power transfer (MCR-WPT) system attains the maximum value at two frequencies splitting in an over-coupled region. To achieve suitable transfer characteristics, impedance compensation methods have been used in MCR-WPT domain. In securing the constant output power and transfer efficiency in a constant frequency mode, a topology of the MCR-WPT system with two transmitting coils is employed. First, the circuit model is designed while evaluating the transmission characteristics. Second, when the two transmitting coils are placed into the transmitting loop, the main transmitter and sub-transmitter loops are created by sharing the same transmitter. The use of two transmitting coils to achieve a magnetic field superposition is investigated. Constant output power and transfer efficiency are then investigated in a constant frequency mode. Finally, the experimental equipment is designed. Experimental results confirm the effectiveness and robustness of the topology. Such a topology can be optimized for the transfer performance by itself and can achieve constant output power and transfer efficiency. If the distance between the two transmitting coils is appropriate and the receiving coil moves between the two transmitting coils, the fluctuation of the output power and transfer efficiency of the MCR-WPT system is less than 5%.

1. INTRODUCTION

Nikola Tesla is known as the first researcher who conducted wireless power transfer experiment in the early 20th century [1]. From then on, considerable progress has been made in the field of wireless power transfer. The technologies include inductive power transfer [2, 3], electrical-field coupled wireless power transfer [4, 5], magnetic coupling resonance wireless power transfer (MCR-WPT) [6, 7], microwave wireless power transfer [8], etc. MCR-WPT technology was introduced in 2007 [9], and it has attracted much attention in conducting several studies and developing different applications [10].

In an over-coupled region, frequency splitting occurs in MCR-WPT systems [7]. Also, the vibration phenomena of receiving and relay coils are found in a three-coil MCR-WPT system, respectively [11, 12]. Thus, MCR-WPT system is quite sensitive to both alignment and distance changes between coils. Any change in the coil position from the initial optimal location leads to declining transfer efficiency [13]. As noted, the output power and transfer efficiency are maximized if the system satisfies the optimal impedance matching condition [14–17]. In [18], uncertainty usually exists in MCR-WPT systems for moving objects. To enhance the robustness of the uncertain parameter variations, a modified MCR-WPT system structure and an interval-based uncertain optimization method are suggested. However, two tuning and impedance matching circuits are used to compensate the reactive power in the MCR-WPT system. The optimization method has become more complicated. In [19], the mechanism of the

Received 7 January 2019, Accepted 4 April 2019, Scheduled 30 May 2019
* Corresponding author: Suqi Liu (liusuqi2009@126.com).
[1] School of Mechanical and Electrical Engineering, Guilin University of Electronic Technology, Guilin, Guangxi 541004, China.
[2] Key Laboratory of High Performance Complex Manufacturing, Central South University, Changsha 410083, China.

impedance compensation evaluated in an MCR-WPT system which includes two compensation coils. This paper uses impedance compensation to adjust the magnetic field and further modify the reactive and active powers of the MCR-WPT system. However, it is difficult to employ this topology in any application because the transfer distance of the two compensation coils is adjusted manually. In [18], a mechanism of the dynamic impedance compensation for MCR-WPT is recommended by employing a compensator. Simultaneously, it attains the maximum output power and transfer efficiency in constant frequency mode. The scheme of the dynamic compensation for MCR-WPT using a compensator is convenient to attain the dynamic impedance compensation. This can be done by adding or eliminating capacitances or inductances from the compensator. However, adding or getting rid of capacitances or inductances from the compensator will bring a transient impact of the MCR-WPT system. Therefore, the initial methods used have drawbacks in practical applications.

In this study, an efficient topology is recommended. Also, this study focuses on two transmitting coils to achieve magnetic field superposition and ultimately, attain constant output power and transfer efficiency. First, the circuit model is established, and transmission characteristics are analyzed. Second, output power and transfer efficiency are simulated using the Biot-Savart law [21] and MATLAB software. Third, the experimental equipment of a MCR-WPT system is created. By comparing the simulated and experimental results, the topology can be optimized in the transmission performance by itself. By doing so, the constant output power and transfer efficiency are achieved in constant frequency mode.

2. THEORETICAL ANALYSIS

Figure 1 presents the MCR-WPT system model with the two transmitting coils to obtain the constant output power and transfer efficiency. Figure 1(a) shows a sketch that involves the two transmitting coils L_1 and L_3. The two transmitting coils are placed into a transmitting loop. The main transmitter and sub-transmitter loops are then designed by sharing the same circuit of the transmitter, as shown in Figure 1(b). U_S is the high-frequency power supply; R_S is the internal resistance; R_1, R_2, and R_3 are the equivalent resistances; L_1, L_2, and L_3 are the self-inductances of the coils; C_1, C_2, and C_3 are the resonant capacitors; R_L is the equivalent load resistance. Meanwhile, d_1 is the transfer distance between the main transmitting and receiving coils; d_2 is the transfer distance between the sub-transmitting and receiving coils; and $d_3 = d_1 + d_2$ is the transfer distance between the main transmitting and sub-

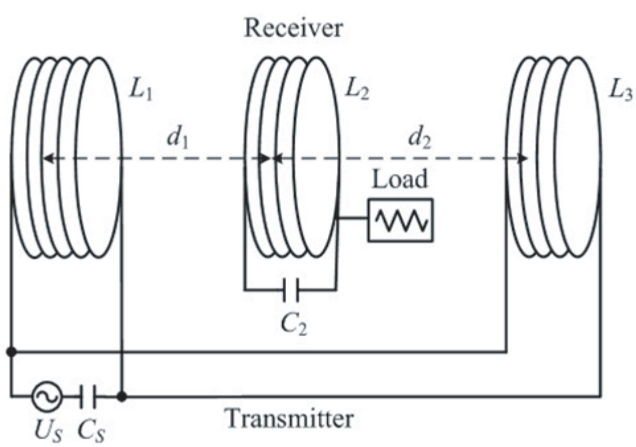

(a)

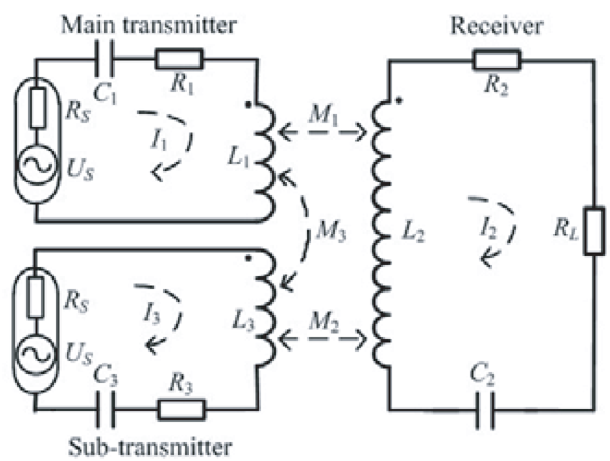

(b)

Figure 1. The MCR-WPT system model with two transmitting coils to obtain constant output power and transfer efficiency. (a) The sketch of the MCR-WPT system with two transmitting coils L_1 and L_3. (b) The equivalent circuit of the MCR-WPT system that involves the main transmitter, sub-transmitter, and receiver loops. When the two transmitting coils are placed into the transmitting loop, the main transmitter and sub-transmitter loops are created by sharing the same circuit of the transmitter.

transmitting coils. M_1, M_2, and M_3 are mutual inductances. At the L_1 coil side, $M_1 > M_2 > M_3$; at the L_3 coil side, $M_2 > M_1 > M_3$; at the middle of the L_1 and L_3 coils, $M_1 \approx M_2 > M_3$. For the analysis, M_3 is neglected because M_1 and M_2 are much larger.

In general, it is assumed that $C_S = C_1 = C_2 = C_3 = C$, $L_1 = L_2 = L_3 = L$, $R_2 + R_L = R$, $R_L = \beta R$, $R_1 + R_S = R_3 + R_S = \sigma R$ (where σ is the ratio of the resistances of the main transmitting or sub-transmitting and receiving coils, $\sigma > 0$); the frequency detuning factor of the main transmitter, sub-transmitter, and receiver is $\xi = Q_0(\omega/\omega_0 - \omega_0/\omega)$; the quality factor of the main transmitter, sub-transmitter, and receiver is $Q_0 = \omega_0 L/R = 1/(\omega_0 < CR)$; the resonance angular frequencies of the main transmitter, sub-transmitter, and receiver are $\omega_0 = 1/(LC)^{0.5}$; and the resonance frequencies of the main transmitter, sub-transmitter, and receiver are $f_0 = \omega_0/(2\pi)$.

Figure 1 shows the MCR-WPT system with a driving source of angular frequency ω, where Kirchhoff's voltage law is applied to determine the currents in each resonant circuit as shown in Equation (1), where the self-impedance of the main transmitter Z_1, sub-transmitter Z_3, and receiver Z_2 is expressed as Equation (2) [19].

$$\begin{cases} Z_1 I_1 - j\omega M_1 I_2 = U_S \\ Z_2 I_2 - j\omega M_1 I_1 - j\omega M_2 I_3 = 0 \\ Z_3 I_3 - j\omega M_2 I_2 = U_S \end{cases} \tag{1}$$

$$\begin{cases} Z_1 = Z_3 = R_1 + R_S + j\omega L_1 + \dfrac{1}{j\omega C_1} \\ = \left(\sigma + \dfrac{j\omega_0 L}{R}\dfrac{\omega}{\omega_0} + \dfrac{1}{j\omega_0 CR}\dfrac{\omega_0}{\omega}\right) R = (\sigma + j\xi)R \\ Z_2 = R_2 + R_L + j\omega L_2 + \dfrac{1}{j\omega C_2} \\ = \left(1 + \dfrac{j\omega_0 L}{R}\dfrac{\omega}{\omega_0} + \dfrac{1}{j\omega_0 CR}\dfrac{\omega_0}{\omega}\right) R = (1 + j\xi)R \end{cases} \tag{2}$$

Based on [20], the impedance coupling factors τ_1 and τ_2 can be shown as Equation (3), which indicates the ability of the impedance coupling.

$$\begin{cases} \tau_1 = \dfrac{\omega M_1}{\sqrt{(R_1 + R_S)(R_2 + R_L)}} = \dfrac{\omega M_1}{\sqrt{\sigma}R}, \quad \tau_1 \geq 0 \\ \tau_2 = \dfrac{\omega M_2}{\sqrt{(R_1 + R_S)(R_2 + R_L)}} = \dfrac{\omega M_2}{\sqrt{\sigma}R}, \quad \tau_2 \geq 0 \end{cases} \tag{3}$$

In Equations (1), (2), and (3), the currents of the main transmitter, sub-transmitter, and receiver coils are

$$\begin{cases} I_1 = \dfrac{(1 + j\xi)(\sigma + j\xi) + \sigma\tau_2^2 - \sigma\tau_1\tau_2}{(1 + j\xi)(\sigma + j\xi)^2 + \sigma(\sigma + j\xi)(\tau_1^2 + \tau_2^2)}\dfrac{U_S}{R} \\ I_2 = j\dfrac{\sqrt{\sigma}(\sigma + j\xi)(\tau_1 + \tau_2)}{(1 + j\xi)(\sigma + j\xi)^2 + \sigma(\sigma + j\xi)(\tau_1^2 + \tau_2^2)}\dfrac{U_S}{R} \\ I_3 = \dfrac{(1 + j\xi)(\sigma + j\xi) + \sigma\tau_1^2 - \sigma\tau_1\tau_2}{(1 + j\xi)(\sigma + j\xi)^2 + \sigma(\sigma + j\xi)(\tau_1^2 + \tau_2^2)}\dfrac{U_S}{R} \end{cases} \tag{4}$$

According to the root mean square (RMS) current I_2 of the receiving coil, the output power is $P_{out} = |I_2|^2 R_L$. Letting $\partial P_{out}/\partial\xi = 0$, we obtain three roots: $\xi_1 = 0$, $\xi_2 = -(2\sigma + \sigma^2 + \sigma\tau_1^2 + \sigma\tau_2^2)^{0.5}$, and $\xi_3 = (2\sigma + \sigma^2 + \sigma\tau_1^2 + \sigma\tau_2^2)^{0.5}$. If $\xi = 0$, $\tau_1 = 1$, and $\tau_2 \approx 0$, namely, at the critical coupled point [19], the maximum output power is $P_{out\,\max} = (\beta U_S^2)/(4\sigma R)$. Thus, the normalized output power can be expressed as Equation (5). The transfer efficiency can be seen in Equation (6).

$$\psi = \frac{P_{out}}{P_{out\,\max}} = \frac{4\sigma^2(\sigma^2 + \xi^2)(\tau_1 + \tau_2)^2}{[\sigma^2(1 + \tau_1^2 + \tau_2^2) - (1 + 2\sigma)\xi^2]^2 + \xi^2[2\sigma + \sigma^2 + \sigma(\tau_1^2 + \tau_2^2) - \xi^2]^2} \tag{5}$$

$$\eta = \frac{P_{out}}{P_{in}} = \frac{|I_2|^2 R_L}{|I_1|^2 R_1 + |I_2|^2 (R_2 + R_L) + |I_3|^2 R_1}$$
$$= \frac{\beta(\tau_1 + \tau_2)^2(\sigma^2 + \xi^2)}{(\sigma + \sigma\tau_1^2 - \sigma\tau_1\tau_2 - \xi^2)^2 + (\sigma + \sigma\tau_2^2 - \sigma\tau_1\tau_2 - \xi^2)^2 + (\tau_1 + \tau_2)^2(\sigma^2 + \xi^2) + 2(1+\sigma)^2\xi^2} \quad (6)$$

3. SIMULATION ANALYSIS

In physics, the Biot-Savart law relates the magnetic field to the magnitude, direction, length, and proximity of the electric current. This law is fundamental to magnetostatics and plays a similar role to Coulomb's law in electrostatics. The law is valid in the magnetostatic approximation and is consistent with both Ampere's circuital law and Gauss's law for magnetism [21]. Figure 2 shows a sketch of the mutual inductance of the MCR-WPT system with two transmitting coils, which achieves a magnetic field superposition and then achieves constant output power and transfer efficiency.

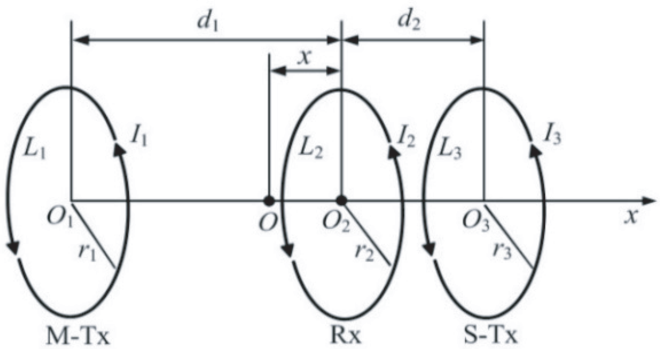

Figure 2. The sketch of the mutual inductance of the MCR-WPT system including two transmitting coils to obtain the magnetic field superposition and then achieves constant output power and transfer efficiency. The sketch includes the main transmitting coil (M-Tx) L_1, sub-transmitting coil (S-Tx) L_2, and receiving coil (Rx) L_3.

Based on the Biot-Savart law, the induction intensity of the circular coil L_1 at the position of the coil L_2 is equal to $B_1 = \mu_0(n_1n_2)^{0.5}r_1^2 I_1/(2(r_1^2 + d_1^2)^{3/2})$; the induction intensity of the circular coil L_3 at the position of the coil L_2 equals $B_2 = \mu_0(n_2n_3)^{0.5}r_3^2 I_3/(2(r_3^2 + d_2^2)^{3/2})$, where $\mu_0 = 4\pi \times 10^{-7}$ H/m is the permeability of vacuum; r_1, r_2, and r_3 are the radii of the M-Tx, S-Tx, and Rx coils, respectively. n_1, n_2, and n_3 are the turn numbers of the M-Tx, S-Tx, and Rx coils, respectively; O is the central point between the M-Tx and S-Tx coils; O_1, O_2, and O_3 are the geometric centers of the M-Tx, S-Tx, and Rx coils, respectively; x is the distance between points O_2 and O; this is a variable value. Φ_1 represents the magnetic flux of the magnetic field excited by the coil L_1 through the coil L_2; Φ_2 represents the magnetic flux of the magnetic field excited by the coil L_3 through the coil L_2; and the other parameters were defined previously and are shown in Figure 1. Thus, M_1 and M_2 can be written as

$$\begin{cases} M_1 = \dfrac{\Phi_1}{I_1} = \dfrac{\pi r_2^2 B_1}{I_1} = \dfrac{\pi\mu_0(n_1n_2)^{0.5}(r_1r_2)^2}{2(r_1^2 + d_1^2)^{3/2}} \\ M_2 = \dfrac{\Phi_2}{I_3} = \dfrac{\pi r_2^2 B_2}{I_3} = \dfrac{\pi\mu_0(n_2n_3)^{0.5}(r_2r_3)^2}{2(r_3^2 + d_2^2)^{3/2}} \end{cases} \quad (7)$$

According to Equations (3) and (7), the impedance coupling factors τ_1 and τ_2 in Equation (3) can also be written as

$$\begin{cases} \tau_1 = \dfrac{\pi\omega\mu_0(n_1n_2)^{0.5}(r_1r_2)^2}{2\sqrt{\sigma}R(r_1^2+d_1^2)^{3/2}} = \dfrac{\pi\omega\mu_0(n_1n_2)^{0.5}(r_1r_2)^2}{2\sqrt{\sigma}R\left(r_1^2+\left(\dfrac{d_1+d_2}{2}+x\right)^2\right)^{3/2}}, & \tau_1 > 0 \\ \tau_2 = \dfrac{\pi\omega\mu_0(n_2n_3)^{0.5}(r_2r_3)^2}{2\sqrt{\sigma}R(r_3^2+d_2^2)^{3/2}} = \dfrac{\pi\omega\mu_0(n_2n_3)^{0.5}(r_2r_3)^2}{2\sqrt{\sigma}R\left(r_3^2+\left(\dfrac{d_1+d_2}{2}-x\right)^2\right)^{3/2}}, & \tau_2 > 0 \end{cases} \tag{8}$$

Based on Figures 1 and 2, the transfer distances, $d_3 = d_1 + d_2$, are assumed constant with the values being 32 mm and 45 mm, respectively. When the receiving coil L_2 shifts from the main transmitting coil L_1 to the sub-transmitting coil L_3, the transfer distances, $d_2 = d_3 - d_1$, are the variables. Thus, in Equations (5), (6), and (8), including the simulation parameters in Table 1, the output power and transfer efficiency are plotted in Figure 3. In addition, cited in Equations (5), (6), and Table 1, with the given $\tau_2 = 0$, the MCR-WPT system is converted into a two-coil MCR-WPT system as the energy exchange mainly occurs at L_1 and L_2 but not at L_2 and L_3. The normalized output power is seen in Figure 4(a), and the transfer efficiency of the MCR-WPT system is shown in Figure 4(b). Coils L_1 and L_2 are symmetrical in space, where the transfer characteristics of the MCR-WPT system can be obtained through the superposition principle [19, 20].

Table 1. The simulation parameters of the output power and transfer efficiency.

Parameter	M-Tx	S-Tx	Rx
Frequency f_0/kHz	140	140	140
Inductance L/μH	29.25	29.25	29.25
Capacitance C/nF	44.18	44.18	44.18
Radius r/m	23×10^{-3}	23×10^{-3}	23×10^{-3}
Number of turns n	20	20	20
Distance $d_3 = d_1 + d_2$/m	32×10^{-3} or 45×10^{-3}		
Material	Copper	Copper	Copper
Impedance scaling factor σ	0.5	0.5	
Frequency detuning factor ξ		0.262 or 0.36	
Load R_L/Ω			1

In Figures 3(a) and 3(b), in the parallel mode, the output power of point O_2 can be obtained by adding up the output power of the points O_1 and O_3 and should be superimposed in the parallel mode because the main transmitting and sub-transmitting coils are connected in parallel. The output power of point O_2 is then obtained. Between points O_1 and O_3, the output power of point O increases from the minimum to the maximum value as transfer distance d_3 decreases. Outside points O_1 and O_3, the output power dramatically declines. Similarly, in Figures 3(c) and 3(d), the trends in the transfer efficiency are similar to those of the output power of the MCR-WPT system.

In Figure 4(a), the normalized output power relates to parameters σ, ξ, and τ_1. There are three states: (1) under coupling region, (2) critical coupling point, and (3) over-coupling region. At the under coupling region ($\tau_1 < 1$), the normalized output power decreases right away. In the critical coupling region ($\tau_1 = 1$), the normalized output power achieves the maximum value. Meanwhile, in the over-coupling region ($\tau_1 > 1$), the normalized output power highlights the frequency splitting. Based on the frequency detuning factor $\xi = Q_0(\omega/\omega_0 - \omega_0/\omega)$, the maximum output power is attained at the two splitting angular frequencies ω_1 and ω_2, which belong to a lower frequency mode (LFM) and a higher frequency mode (HFM), respectively.

Similarly, in Figure 4(b), the maximum of the transfer efficiency is obtained at the resonance angular frequency. The transfer efficiency of the MCR-WPT system gradually increases as the parameter τ_1 increases.

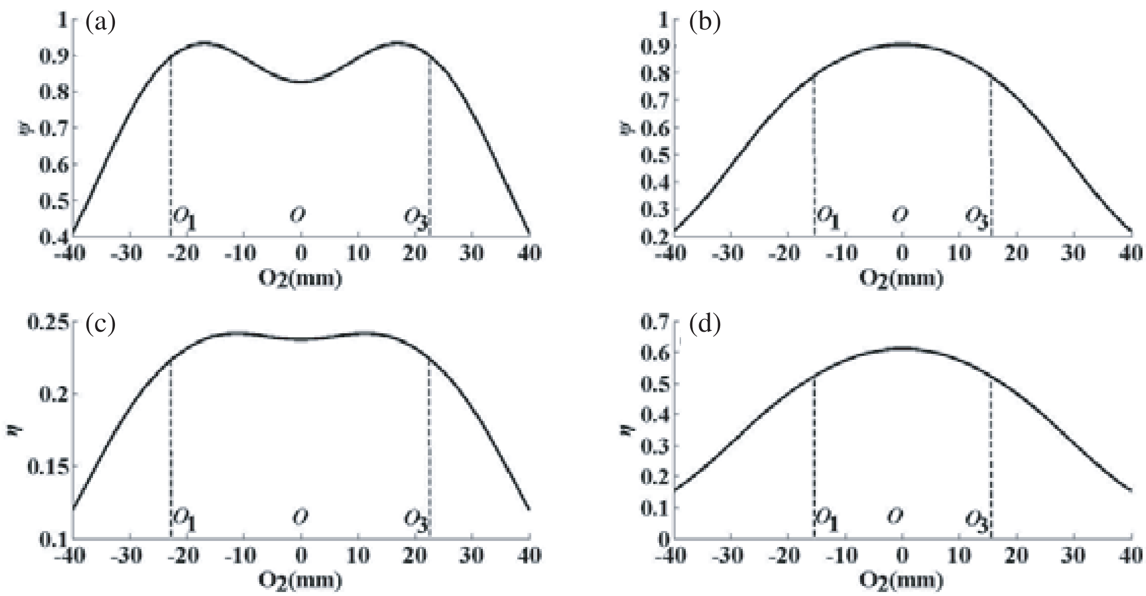

Figure 3. The normalized output power and transfer efficiency of the MCR-WPT system using the magnetic field superposition principle. (a) $\xi = 0.262$, $d_3 = 45\,\text{mm}$, (b) $\xi = 0.36$, $d_3 = 32\,\text{mm}$, (c) $\xi = 0.262$, $d_3 = 45\,\text{mm}$, (d) $\xi = 0.36$, $d_3 = 32\,\text{mm}$.

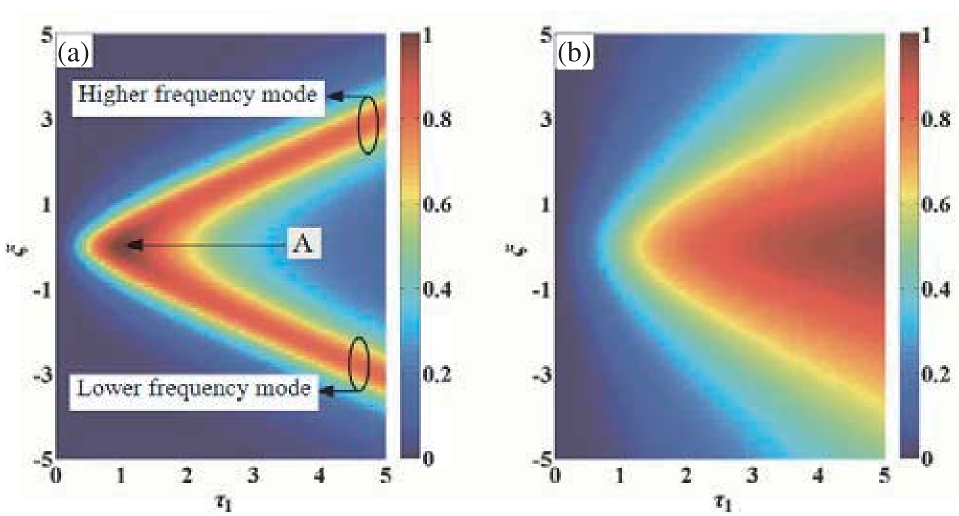

Figure 4. The normalized output power and transfer efficiency of the MCR-WPT system. (a) Normalized output power of the system when $\sigma = 0.5$, $\tau_2 = 0$; (b) Transfer efficiency of the system when $\beta = 1$, $\tau_2 = 0$.

In the above analysis, the following analyses can be made. At point O_1 or O_3, characteristics of the MCR-WPT system mainly depend on characteristics of the two-coil system. At the central point O, characteristics of the MCR-WPT system are obtained by using the synthetic characteristics of points O_1 and O_3. In general, in Figures 3(a) and 3(b), on the x-axis (transfer distance d_3), the output power and transfer efficiency of the MCR-WPT system exhibit characteristics of the superposition. However, in Figures 3(c) and 3(d), on the ξ-axis, the output power of the MCR-WPT system showcases the two peaks in the over coupled region while the transfer efficiency obtains the maximum value at a resonance angular frequency.

Based on [19] and [20], in the over coupled region, the maximum output power of the two-coil system is achieved at the two angular frequency splitting ω_1 and ω_2, which belong to an LFM and an HFM, respectively (see Figure 4(a)).

According to the theory and simulation analysis, in the LFM or HFM, when the receiving coil randomly moves between the main transmitting and sub-transmitting coils, the system will always have constant output power and transfer efficiency at a constant angular frequency ω_L or ω_H using the two transmitting coils. In turn, this achieves the magnetic field superposition and further achieves constant output power and transfer efficiency. Next, the following results are verified in detail in the experiments.

4. EXPERIMENTAL RESULTS

Figure 5 shows the MCR-WPT experimental equipment, including power amplifier, wave generator, oscilloscope, voltage probes, capacitances, transmitter, receiver, load, and main transmitting, sub-transmitting, and receiving coils. Table 1 identifies parameters of the main transmitter, sub-transmitter, and receiver. Then, experimental research is carried out.

In the experiments, the transfer distance between the main transmitting and sub-transmitting coils is assigned, where d_3 is constant, and the values are 20 mm, 30 mm, and 36 mm, respectively. The transfer distance between the main transmitting and receiving coils d_1 is also constant, and the values are 10 mm, 15 mm, and 18 mm. Subsequently, the input voltage and output voltage are measured at different driving frequencies. Similarly, the input and output currents are also measured. Figures 6 and 7 are obtained using these data. In Figure 6, in transferring the distance of the main transmitting

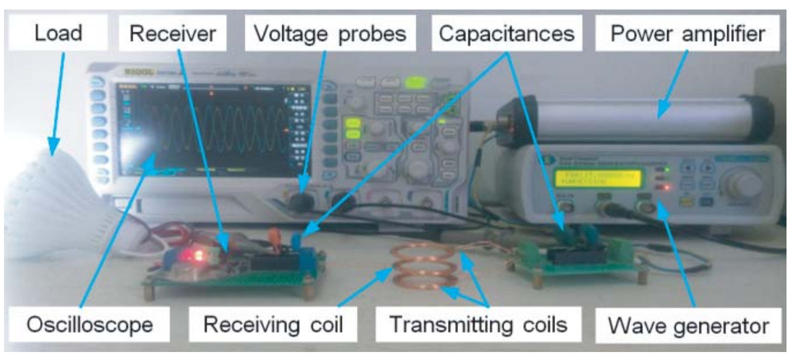

Figure 5. The experimental equipment that use the two transmitting coils to achieve the magnetic field superposition and the constant output power and transfer efficiency.

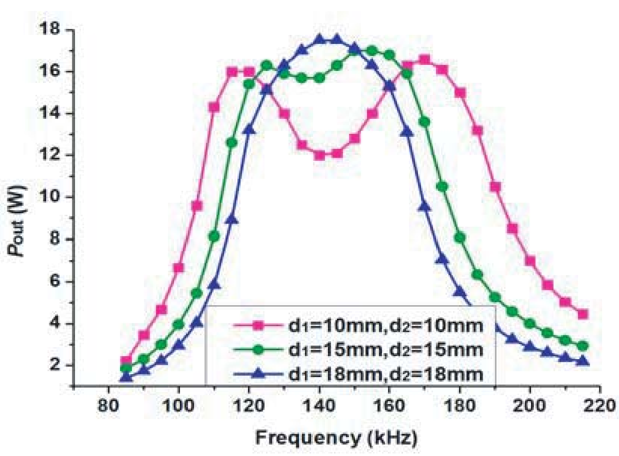

Figure 6. The output power of the system with different driving frequencies.

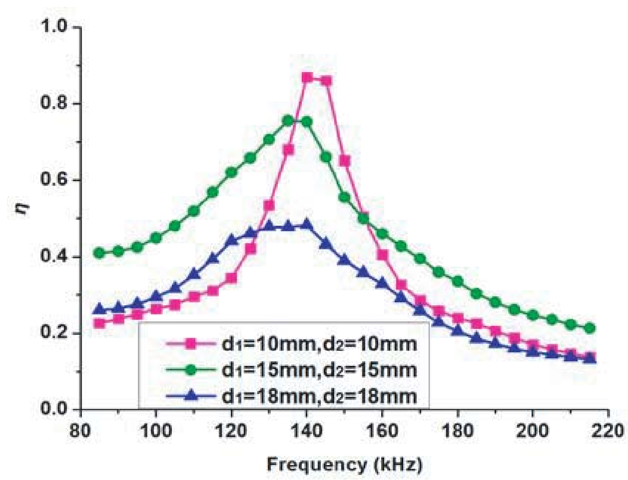

Figure 7. The transfer efficiency of the system with different driving frequencies.

and sub-transmitting coils d_3 is equal to 20 mm, while the output power peaks of the MCR-WPT system appear at the frequencies of 115 kHz and 170 kHz, respectively. When transfer distance d_3 is equal to 30 mm, the output power peaks of the MCR-WPT system appear at the frequencies of 125 kHz and 155 kHz. When transfer distance d_3 is equal to 36 mm, the MCR-WPT system shows the output power peak at the frequency of 140 kHz. In Figure 7, when transfer distance d_3 is equal to 20 mm, 30 mm, and 36 mm, respectively, the system attains the maximum transfer efficiency at the frequency of 140 kHz. When transfer distance d_3 decreases, the transfer efficiency increases. The transfer efficiency curves shift to the higher frequency direction.

Based on the experimental results, when $d_3 = 20$ mm, the output power of the MCR-WPT system takes the maximum values at the frequencies of 115 kHz and 170 kHz. When $d_3 = 30$ mm, the output power obtains the maximum values at the frequencies of 125 kHz and 155 kHz; when $d_3 = 36$ mm, the output power obtains the maximum value at the frequency 140 kHz. The driving source of frequency is moved to these frequencies, then these frequencies keep constant values when the system works. When transfer distance d_3 is constant, the input and output voltages are measured at a different transfer distance d_1 (namely, the receiving coil moves from the main transmitting coil to the sub-transmitting coils). The input and output currents are also evaluated. These are shown in Figures 8 and 9. In the LFM (namely, $d_3 = 20$ mm, $f = 115$ kHz; $d_3 = 30$ mm, $f = 125$ kHz; $d_3 = 36$ mm, $f = 140$ kHz), it is seen that the output power and transfer efficiency achieve a nearly constant value as transfer distance d_1 increases; the fluctuation of the output power and transfer efficiency is less than 5%. However, in higher frequency mode (namely, $d_3 = 20$ mm, $f = 170$ kHz; $d_3 = 30$ mm, $f = 155$ kHz), when transfer distance d_1 increases, the output power dramatically decreases, and the transfer efficiency achieves the minimum value at point O. The experimental results show that different reasons are identified: the power of the transmitter side achieves the maximum value at point O; near the point of maximum output power, anti-phase currents occur in the main transmitting and receiving coils [7]; when the receiving coil moves away a certain distance from the central point O, the phase between the main transmitting and receiving coils is suddenly reversed and changes from anti-phase to in-phase. The power superposition mechanism is described in [19]. This has the effect where reactive powers of the transmitter and receiver sides cause an increase in the reactive power and a decrease in the active power. Thus, phase inversion leads to a sharp decline in performance.

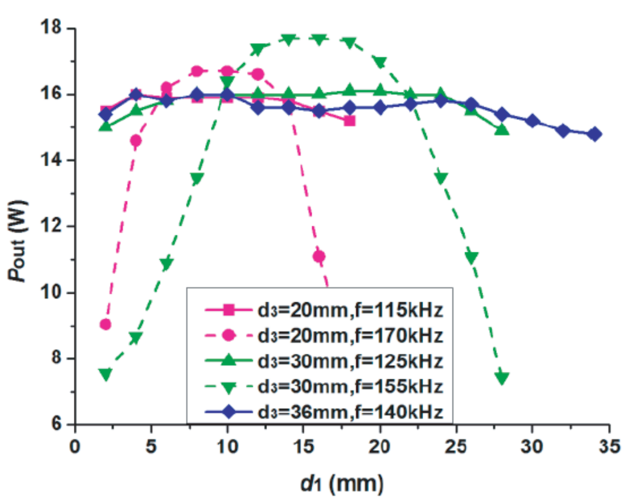

Figure 8. The output power of the system with different transfer distances.

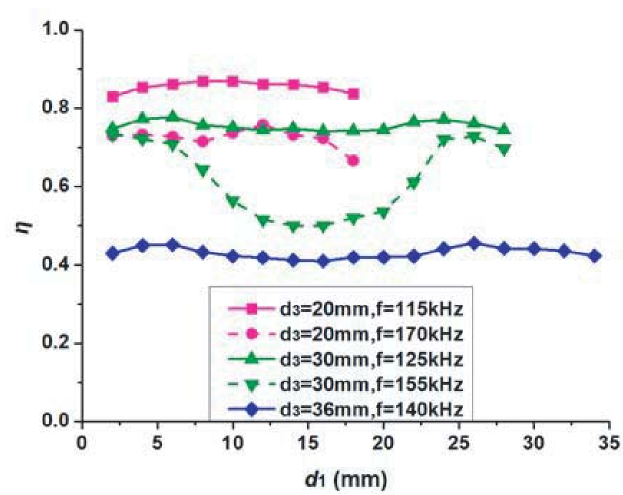

Figure 9. The transfer efficiency of the system with different transfer distances.

In summary, the experimental results are consistent with the simulated ones. In the LFM, when transfer distance d_3 is constant and transfer distance d_1 changes, the MCR-WPT system achieves constant output power and transfer efficiency in the constant frequency mode due to the mechanism of the magnetic field superposition to attain the uniform magnetic field [22].

5. DISCUSSION

When a receiving coil is placed between the two transmitting coils, there are space limits. The receiving coil only shifts between the two transmitting coils. However, in Figure 10, the rail guide vehicle may achieve constant output power and transfer efficiency when it moves on the rail guide. So this topology may provide a practical solution. In any case, using the two transmitting coils to achieve a uniform magnetic field and then to achieve the constant output power of the MCR-WPT system is a good idea. The results of this study may help researchers to find an approach that achieves constant output power and transfer efficiency in open areas, such as charging pads. It is believed that this study will accelerate the practical adaptations of wireless power transfer.

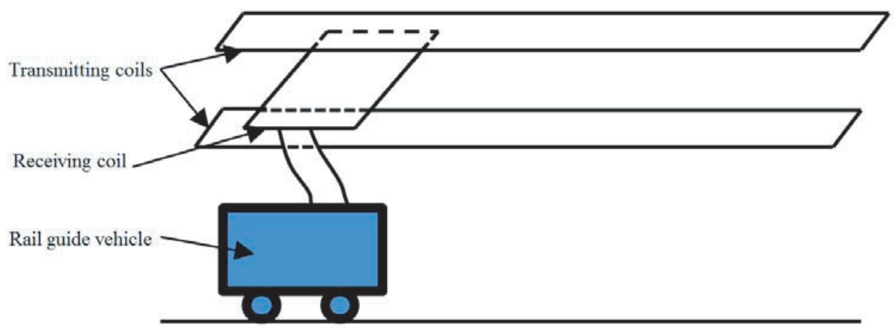

Figure 10. The rail guide vehicle achieves constant output power and transfer efficiency when it moves on the rail guide.

6. CONCLUSION

This paper provides an analysis and simulation of the transfer characteristics of MCR-WPT system by applying the magnetic field superposition principle. In the LFM, the MCR-WPT system with two transmitting coils achieves magnetic field superposition and further attains constant output power and transfer efficiency in constant frequency mode. If the distance between the two transmitting coils is appropriate and the receiving coil moves between the two transmitting coils, the fluctuation of the output power and transfer efficiency of the MCR-WPT system is less than 5%. In the HFM, when the receiving coil moves a certain distance away from the central point, the phase between the main transmitting and receiving coils is suddenly reversed. This phase inversion leads to a sharp decline in performance.

ACKNOWLEDGMENT

This study was supported by the National Key Basic Research Program of China (No. 2014CB049405).

REFERENCES

1. Tesla, N., "Electrical energy," U.S. Patent 1,119,732, Dec. 1, 1914.
2. Bosshard, R. and J. W. Kolar, "Inductive power transfer for electric vehicle charging: Technical challenges and tradeoffs," *IEEE Power Electronics Magazine*, Vol. 3, 22, 2016.
3. Covic, G. A., J. T. Boys, M. L. G. Kissin, et al., "A three-phase inductive power transfer system for roadway-powered vehicles," *IEEE Transactions on Industrial Electronics*, Vol. 54, 3370, 2007.
4. Ishihara, M., K. Umetani, H. Umegami, et al., "Quasi-duality between SS and SP topologies of basic electric-field coupling wireless power transfer system," *Electronics Letters*, Vol. 52, 2057, 2016.

5. Al-Kalbani, A. I., M. R. Yuce, and J. M. Redoute, "A biosafety comparison between capacitive and inductive coupling in biomedical implants," *IEEE Antennas and Wireless Propagation Letters*, Vol. 13, 1168, 2014.
6. AndréKurs, K. A., R. Moffatt, et al., "Wireless power transfer via strongly coupled magnetic resonances," *Science*, Vol. 317, 83, 2007.
7. Sample, A. P., D. T. Meyer, and J. R. Smith, "Experimental results, and range adaptation of magnetically coupled resonators for wireless power transfer," *IEEE Transactions on Industrial Electronics*, Vol. 58, 544, 2011.
8. Brown, W. C., "The history of power transmission by radio waves," *IEEE Transactions on Microwave Theory Techniques*, Vol. 32, 1230, 1984.
9. Karalis, A., J. D. Joannopoulos, and M. Soljačić, "Efficient wireless non-radiative mid-range energy transfer," *Annals of Physics*, Vol. 323, 34, 2006.
10. Hui, S. Y. R., W. Zhong, and C. K. Lee, "A critical review of recent progress in mid-range wireless power transfer," *IEEE Transactions on Power Electronics*, Vol. 29, 4500, 2014.
11. Liu, S., J. Tan, and X. Wen, "Modeling of coupling mechanism of wireless power transfer system and vibration phenomenon of receiver-coil in three-coil system," *AIP Advances*, Vol. 7, 115107, 2017.
12. Liu, S. and J. Tan, "Study on the vibration mechanism of the relay coil in a three-coil WPT system," *Progress In Electromagnetics Research M*, Vol. 70, 117–126, 2018.
13. Huang, R., B. Zhang, D. Qiu, et al., "Frequency splitting phenomena of magnetic resonant coupling wireless power transfer," *IEEE Transactions on Magnetics*, Vol. 50, 1, 2014.
14. Lee, J., Y. Lim, H. Ahn, et al., "Impedance-matched wireless power transfer systems using an arbitrary number of coils with flexible coil positioning," *IEEE Antennas and Wireless Propagation Letters*, Vol. 13, 1207, 2014.
15. Xiao, C., "New insight of maximum transferred power by matching capacitance of a wireless power transfer system," *Energies*, Vol. 10, 688, 2017.
16. Peng, L., O. Breinbjerg, and N. A. Mortensen, "Wireless energy transfer through non-resonant magnetic coupling," *Journal of Electromagnetic Waves and Applications*, Vol. 24, 1587, 2010.
17. Peng, L., J. Y. Wang, L. X. Ran, et al., "Performance analysis and experimental verification of mid-range wireless energy transfer through non-resonant magnetic coupling," *Journal of Electromagnetic waves and Applications*, Vol. 25, 845, 2011.
18. Luo, Y., Y. Yang, X. Wen, et al., "Enhancing the robustness of the wireless power transfer system to uncertain parameter variations using an interval-based uncertain optimization method," *Energies*, Vol. 11, 2032, 2018.
19. Liu, S., J. Tan, and X. Wen, "Dynamic impedance compensation for wireless power transfer using conjugate power," *AIP Advances*, Vol. 8, 025210, 2018.
20. Liu, S. and J. Tan, "Dynamic impedance compensation for WPT using a compensator in a three-coil wireless power transfer system," *Circuit World*, Vol. 44, No. 4, 171, 2018.
21. Biot-Savart law, https://en.wikipedia.org/wiki/BiotSavart_law.
22. Helmholtz coil, https://en.wikipedia.org/wiki/Helmholtz_coil.